Very High Resolution SAR and Multichannel SAR/MTI

Dr. Patrick Berens
Research Institute for High-Frequency Physics and Radar Techniques (FHR)
Research Establishment for Applied Science (FGAN)
53343 Wachtberg, Germany

berens@fgan.de

ABSTRACT

SAR is widely used today in earth observation and is a potential means for military surveillance. However, systems only operating in the basic SAR mode will be superseded by new developments which fulfil much more user demands. Highest resolution in flight direction combined with a far range operation cannot be reached in stripmap mode. The spotlight mode has to be implemented demanding for special capabilities of the hardware and the data processing chain. To achieve a fine resolution in range direction, transmit signals with very large bandwidth have to be used. Technological imitations force the developers to implement new strategies to acquire the necessary bandwidth.

Multichannel SAR systems offer great advantages compared to the conventional ones. Depending on the antenna configuration such systems allow to measure the height of image pixels or to detect moving objects in the illuminated scene.

1.0 VERY HIGH RESOLUTION SAR

1.1 Relation of resolution and k-set

The analyses of the resolution of a SAR system must distinguish range and azimuth (flight direction) resolution. While a broad bandwidth of the transmitted and received pulses is responsible for a fine range resolution, the azimuth resolution can be improved by using a short wavelength or by a large processing angle. However, in both directions the designated measures cause similar effects in the wave number domain representation of the echo data. Thus, a common examination of the relation between resolution and k-set can be accomplished.

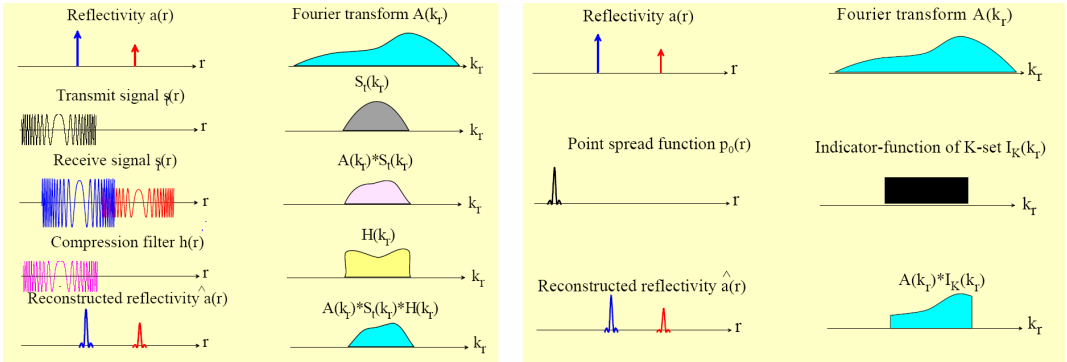

Figure 1: Relation of k-set and image resolution. Left diagram: representation of signals in spatial and wave number domain. Right diagram: Influence of the point spread function.

Berens, P. (2006) Very High Resolution SAR and Multichannel SAR/MTI. In *Advanced Radar Signal and Data Processing* (pp. 8-1 – 8-14). Educational Notes RTO-EN-SET-086, Paper 8. Neuilly-sur-Seine, France: RTO. Available from: http://www.rto.nato.int/abstracts.asp.

Report Documentation Page

Form Approved
OMB No. 0704-0188

1. REPORT DATE	2. REPORT TYPE	3. DATES COVERED
01 SEP 2006	**N/A**	**-**

4. TITLE AND SUBTITLE	5a. CONTRACT NUMBER
Very High Resolution SAR and Multichannel SAR/MTI	5b. GRANT NUMBER
	5c. PROGRAM ELEMENT NUMBER
6. AUTHOR(S)	5d. PROJECT NUMBER
	5e. TASK NUMBER
	5f. WORK UNIT NUMBER
7. PERFORMING ORGANIZATION NAME(S) AND ADDRESS(ES) **Research Institute for High-Frequency Physics and Radar Techniques (FHR) Research Establishment for Applied Science (FGAN) Neuenahrer Str. 20, D-53343 Wachtberg GERMANY**	8. PERFORMING ORGANIZATION REPORT NUMBER
9. SPONSORING/MONITORING AGENCY NAME(S) AND ADDRESS(ES)	10. SPONSOR/MONITOR'S ACRONYM(S)
	11. SPONSOR/MONITOR'S REPORT NUMBER(S)

12. DISTRIBUTION/AVAILABILITY STATEMENT
Approved for public release, distribution unlimited

13. SUPPLEMENTARY NOTES
See also ADM001925, Advanced Radar Signal and Data Processing., The original document contains color images.

14. ABSTRACT

15. SUBJECT TERMS

16. SECURITY CLASSIFICATION OF:			17. LIMITATION OF ABSTRACT	18. NUMBER OF PAGES	19a. NAME OF RESPONSIBLE PERSON
a. REPORT	b. ABSTRACT	c. THIS PAGE			
unclassified	**unclassified**	**unclassified**	**UU**	**14**	

Figure 1 illustrates the relation of signals in the spatial domain and its Fourier correspondences in k- or wave number domain. The left diagram depicts the complete one-dimensional image formation process:

- a given scene will be illuminated using an arbitrary transmit pulse, usually a chirp signal
- reflected echoes of all scene targets, two chirp signals in the example, will be received
- a matched filter is used for compression by a factor determined by the time-bandwidth product of the transmit signal (signal-to-noise-ratio is improved accordingly).

The reconstructed image is the convolution output of the scene and the point spread function. The right diagrams represent a generalized view of the same relationship. The image properties are completely defined by the reflectivity and the point spread function. The concrete appearance of the transmit signal is irrelevant for the imaging process. A corresponding situation results in azimuth direction. A k-set will be generated by observation of the scene from different directions. A large observation angle thus produces a large k-set and a fine azimuth resolution. Since the point spread function is the Fourier correspondence of the indicator function in k-space, it is clear, that the wave number domain has to be covered without gaps. Otherwise, high sidelobes arise in the target response. Figure 2 illustrates the point spread function for different cases of k-sets. Case a) is typical for a SAR with a limited bandwidth. The observation angle is also bounded, perhaps by operation in stripmap mode. K-set acquisition in case b) is done using a monofrequent radar system and an overall observation. Though the bandwidth of the transmit signal is negligible, resolution can be obtained in all directions. Sidelobes increase because of the small proportion of the covered k-area. Case c) depicts the situation of a system with very large relative bandwidth and a wide processing angle. This configuration produces problems in the data processing, because very accurate algorithms have to be used. Diagram d) shows the effect when undersampling occurs in the wave number domain which results in sidelobes. Moreover, the distance of samples in k-space is reciprocal to the image size. If the illuminated scene (according to the antenna beam angle) is larger than this image area, aliasing appears. Compared to this case, the unconformable structure of the k-set in diagram e) leads to reduced sidelobes. However, the integrated sidelobe level remains high. Aliasing can be avoided by this measure. Diagram f) shows a well formed k-set with a superior point spread function.

1.2 Measures to enhance range resolution

1.2.1 Overview of methods

With the increasing demands according to the resolution capability of modern SAR systems, the range resolution encounters limitations. The necessary bandwidth claims for superior Antenna, HF- and central electronics and A/D converter.

Often, the A/D conversion of the received echoes plays a limiting role which also influences the data processing. For a resolution of a decimetre, a bandwidth of 1.5 GHz has to be used. However, even modern A/D converters with adequate quantization offer sampling rates of only 800 MHz. Consequently, a direct sampling of the echoes cannot be realized. Two methods allow to acquire data with the demanded bandwidth.

The deramping is implemented in a couple of current radar systems to reduce the signal bandwidth which has to be recorded. The application is not restricted to SAR, but also ISAR systems like TIRA (tracking and imaging radar) of FGAN apply this method. The idea is to transmit linear frequency modulated pulses and to convert the received echoes using an equivalent modulated reference signal to the base band. If the frequency modulation of the reference signal compensates for the echo modulation, the bandwidth of the acquired signal will be reduced considerably.

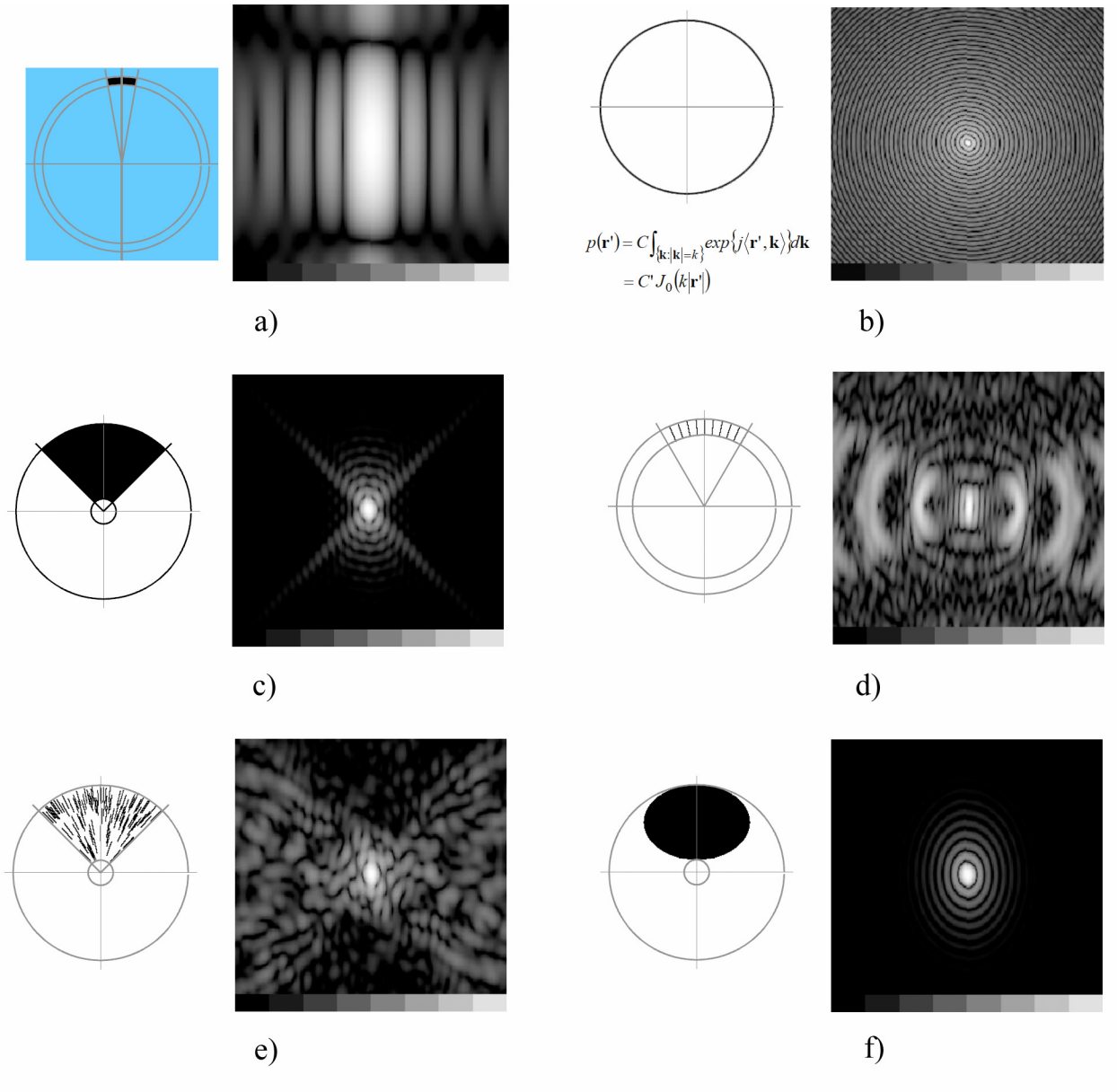

Figure 2:Examples of different shaped k-sets and their corresponding point spread functions. a) small angular sector, small bandwidth, b) Large angular sector, small bandwidth, c) Large angular sector, large bandwidth, d) undersampled observation angle, e) scattered frequency band, f) well formed k-set, tuned frequency bands

The alternative solution is to share the total bandwidth between some pulses having different centre frequencies. These pulses will be transmitted and received subsequently and can be digitized by the available sample rate. In the processing process, the partial signals will be combined coherently.

1.2.2 Deramping

The idea of deramping is to reduce the signal bandwidth within the analogue section of the receiver and to perform the digital signal processing with a low sampling rate. If linear frequency modulated transmit signals will be used the down conversion with an also linear FM reference signal leads to mono-frequent signal contributions. Figure 3 illustrates this subject.

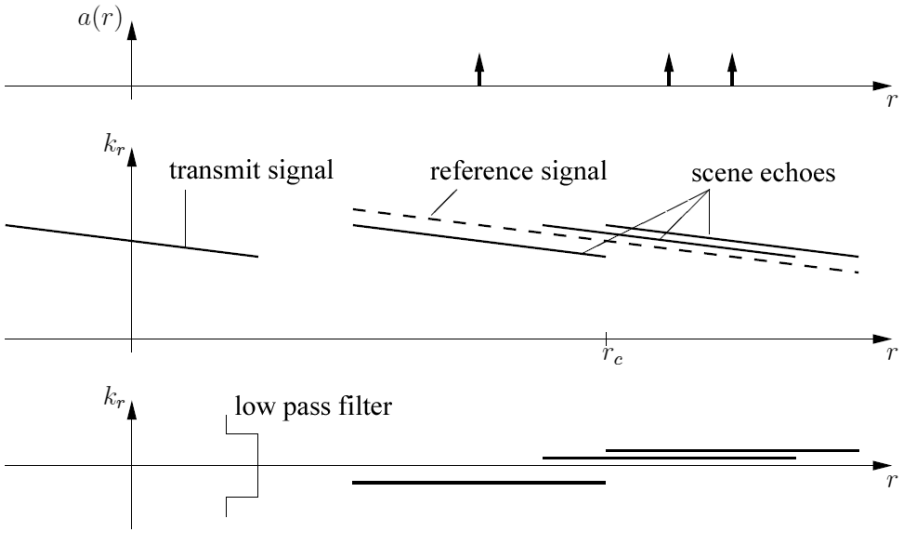

Figure 3: Illustration of the dramping method: The upper diagram represents the reflectivity of a scene having three point scatterers. Beneath, the transmit signal and scene echoes are depicted. The lower diagram shows the received signal after deramping. Now, echoes are mono frequent contributions of the total signal. The indicated low pass filter causes a range limitation.

Some characteristics become clear by this presentation:

- The reference signal must be a scene size larger than the transmit pules.
- The larger the imaged range area should be, the larger the bandwidth of the reference signal has to be chosen.
- After deramping, the total bandwidth is proportional to the scene extension. A low pass filtering of the received signal corresponds to a limitation of the received range interval. The signal bandwidth thus can be adopted to the available samping rate.

Now, we will analyse the deramping mathematically. The linear frequency modulated transmit signal

$$s_t(r) = \text{rect}\left(\frac{r}{K_r/\gamma}\right) e^{j(k_{r,0}r - \frac{\gamma}{2}r^2)}$$

is assumed to be given which covers the interval $\left[k_{r,0} - K_r/2, k_{r,0} + K_r/2\right]$. K_r is the size of the wave number interval and γ denotes the wave number slope in r. The length of the signal is K_r/γ. If this signal will be reflected by a point target with reflectivity α at distance r', the sensor receives the echo

$$z(r) = s_t(r - r') = \alpha\,\text{rect}\left(\frac{r - r'}{K_r/\gamma}\right) e^{j\left[k_{r,0}(r-r') - \frac{\gamma}{2}(r-r')^2\right]}.$$

The deramping will be performed by down-conversion using the reference signal

$$z_{ref}(r) = e^{j\left[k_{r,0}(r-r_c) - \frac{\gamma}{2}(r-r_c)^2\right]},$$

where r_c denotes a reference range within the range of the image. The deramped signal results in

$$\begin{aligned} z_d(r) &= z(r) z_{ref}(r)^* \\ &= \alpha \,\mathrm{rect}\left(\frac{r-r'}{K_r/\gamma}\right) e^{-jk_{r,0}(r'-r_c)} e^{-j\frac{\gamma}{2}(r'^2-r_c^2)} e^{j\gamma(r'-r_c)r}. \end{aligned}$$

The last exponential term possesses a linear phase in r which depends on the location r' of the imaged point target. After a Fourier transform this term causes a shift in the wave number domain. It follows

$$\dot{z}_d(k_r) = \frac{\alpha K_r}{\gamma} e^{-j(k_{r,0}+k_r)(r'-r_c)} e^{-jk_r r_c} e^{j\frac{\gamma}{2}(r'-r_c)^2} \mathrm{si}\left\{\frac{K_r}{2\gamma}(k_r - \gamma(r'-r_c))\right\}.$$

The first exponential term supports the accurate information of the range difference $r' - r_c$ which is the basis for the coherent processing of pulses in flight direction. The second phase term is independent of the object distance and can be compensated easily. The third term, known in the literature as residual video phase, has to be examined and removed, if necessary. An exact solution is given in [2] and an approximation is presented in [15]. Finally, the si-function represents the amplitude and shows that the signal has been compressed. The resolution can be determined to $\delta_r = 2\pi / K_r$ which is the common relation of resolution and the size of the k-set.

1.2.3 Synthetic bandwidth

Another idea to overcome the limitation of the bandwidth is to transmit a series of signals which cover different frequency intervals. The coherent combination of the received echoes leads to the final resolution. The principle of synthetic bandwidth (also denoted as stepped chirp) is depicted in Figure 4.

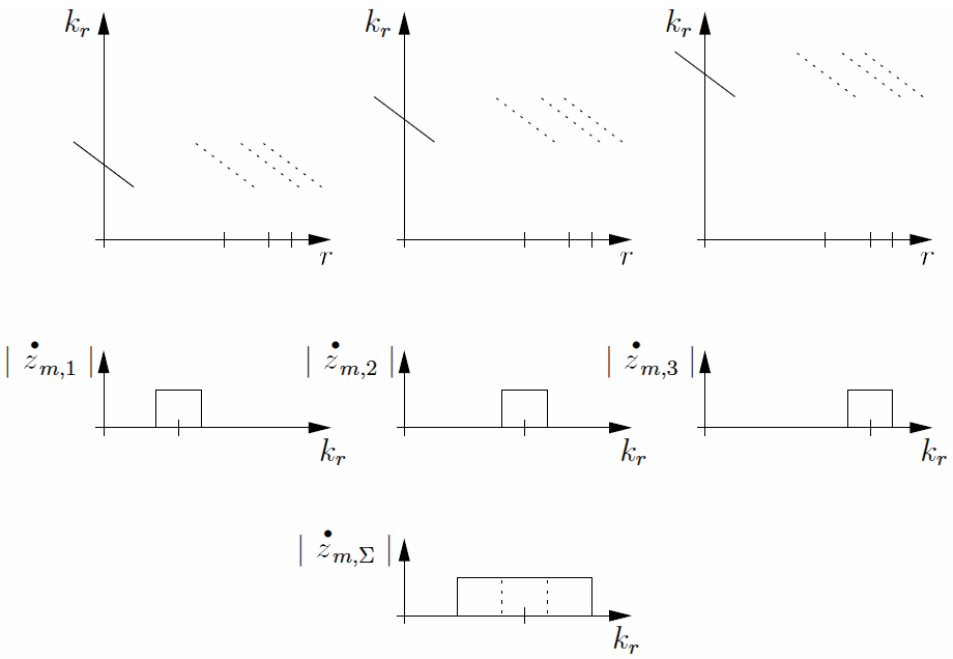

Figure 4: Principle of synthetic bandwidth: The upper images show three transmit signals covering different frequency intervals and their echoes. The second row depicts the spectra. The last diagram shows the combined signal covering the whole wave number interval.

The mathematical analyses starts assuming transmit signals $s_{t,n}(r)$ for $n=1,\ldots\bar{n}$. If $s_{t,n}(r)$ has constant power density $\tilde{L}$ in $\left[k_{r,0}-\bar{n}K_r/2+(n-1)K_r, k_{r,0}-\bar{n}K_r/2+nK_r\right]$ received echoes of a scene with reflectivity $a(r)$ after matched filtering result as

$$\dot{z}_{m,n}(k_r) = \tilde{L}\,\mathrm{rect}\left(\frac{k_r-[k_{r,0}-(\bar{n}-1)K_r/2+(n-1)K_r]}{K_r}\right)\dot{a}(k_r).$$

Coherent superposition leads to

$$\dot{z}_{m,\Sigma}(k_r) = \sum_{n=1}^{\bar{n}}\dot{z}_{m,n}(k_r) = \tilde{L}\,\mathrm{rect}\left(\frac{k_r-k_{r,0}}{\bar{n}K_r}\right)\dot{a}(k_r).$$

The inverse Fourier transformation into the spatial domain results in

$$z_{m,\Sigma}(r) = (p_\Sigma * a)(r), \qquad \text{where} \qquad p_\Sigma(r) = \frac{\tilde{L}\bar{n}K_r}{2\pi}e^{jk_{r,0}r}\mathrm{si}\left\{\frac{\bar{n}K_r}{2}r\right\}$$

is the point spread function. Compared to the resolution of one single pulse (with partial bandwidth) the resolution will be $\delta = 2\pi/(\bar{n}K_r)$, which is enhanced by a factor of $\bar{n}$.

2.0 INTERFEROMETRY

2.1 Two-antenna interferometry

In a conventional SAR image a scene point will be depicted according to its distance to the flight path and the location in flight direction where the point is perpendicular to the synthetic aperture. Thus, reflecting points at circles around the flight path will be located in the result in one single image pixel. It is not possible to localise the point in three dimensions. In terrain height retrieving interferometric SAR (IfSAR) the elevation angle of each ground pixel is estimated by determining the phase difference of the signals from at least two antennas separated along the cross-track direction.

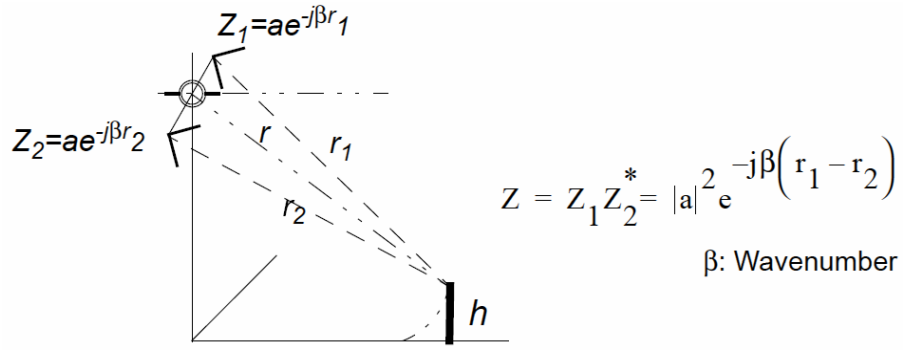

Figure 5: Geometry of single-pass cross-track SAR interferometry.

Figure 5 depicts the geometry for a two antenna configuration. Knowing the ground pixel and the antennas´ positions, the terrain height is obtained from the elevation angle. Due to the 2π ambiguity of this phase difference, a reference point is needed to determine the phase´s principal value and the allowed

terrain height variation is strictly limited. This limitation can be avoided by a suited phase unwrapping procedure (i.e. adding the appropriate number of 2π to each pixel to minimize discontinuities), assuming the terrain slope not to exceed a certain extent, in order to avoid phase aliasing. Due to decorrelation effects this phase unwrapping is an error-prone process, leading partly to poor height estimations. So, phase unwrapping is the key component of SAR interferometry processing, if no digital elevation model is used. Most phase unwrapping algorithms can be categorised into path-following and least-squares algorithms.

An analyses of the k-set of acquired interferometric data shows that a third dimension has also been established in the wave number domain. Figure 6 illustrates this fact. The Fourier counterpart thus incorporates resolution capabilities in all directions.

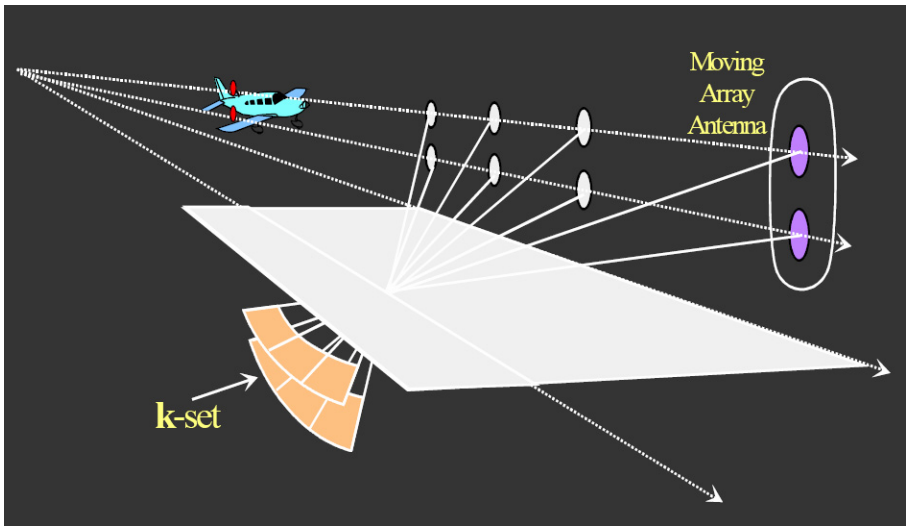

Figure 6: Constellation of interferometric SAR acquisition. The pair of k-sets of the two antennae captures the third dimension in k-space.

A further source for phase corruption is given by contributions of different elevation angles within one resolution cell (so-called layover). Typical problems of that kind rise up in many images with bridges over a valley or a similar constellation. In such a case, the reflectivity of multiple scatterers superpose each other and in the image pixel only the sum of all appears. Hence, the phase which carries the interferometric height information of the pixel is a mixture of the phase of all reflecting elements sharing the same image pixel. If one contribution dominates the others, its height information will prevail. Otherwise, the calculated height will be useless.

Figure 7 depicts an interferometric SAR image which has been recorded using two antennae.

2.2 Multi baseline interferometry

2.2.1 Principle

The height estimation accuracy is inversely proportional to the baseline of the interferometer. But, increasing the baseline results in higher fringe frequencies, thus making the phase unwrapping still harder. Therefore, it is quite natural to reduce these problems by using a multi baseline system: the ambiguities can be removed by a suitable small baseline, thus retrieving the absolute phase with no more need for reference points and phase unwrapping, and the height estimation accuracy can be sustained by a longer baseline. As a second advantage, multi baseline IfSAR allows for estimation of the different elevation angles, caused by mixing different height pixels within one resolution cell, by means of superresolution

methods.

In the literature, some theoretical investigations or simulations of the multi phase centre interferometry can be found [3,9,10].

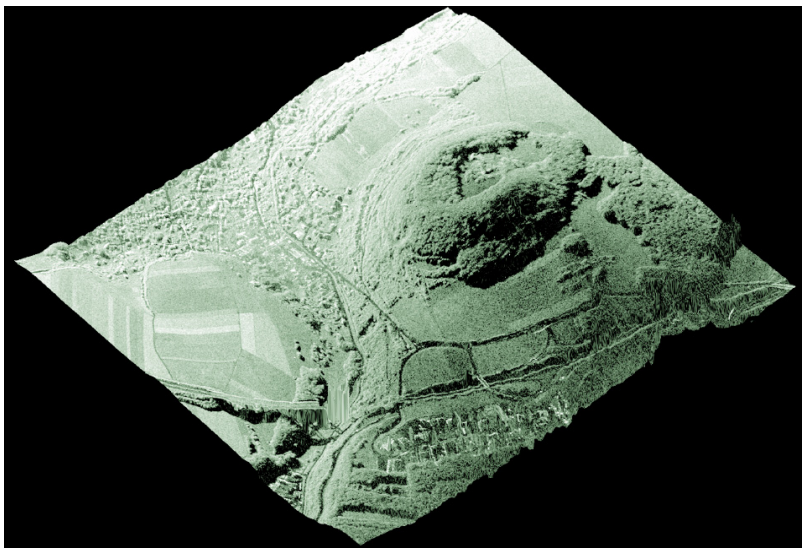

Figure 7: Perspective view of an interferometric SAR image.

Following on, we analyse an antenna configuration with three single antennae separated in cross-track direction. One could expect that a very short baseline results in ambiguity and phase unwrapping removal. On the other hand, we have to minimize the sidelobe level of the three-antenna array, because high sidelobe levels could result in wrong elevation estimates when using noisy data. This minimisation determines the position of the third antenna. Figure 8 depicts the scan pattern of a three-antenna configuration with baseline ratios 1:2:3 compared to a two-antenna configuration. As can be seen the ambituity interval is tripled compared to the two-antenna array. An irrational ratio would in fact result in an infinite ambiguity interval at the cost of increasing sidelobe levels. However, this could only be exploited with noise-free data.

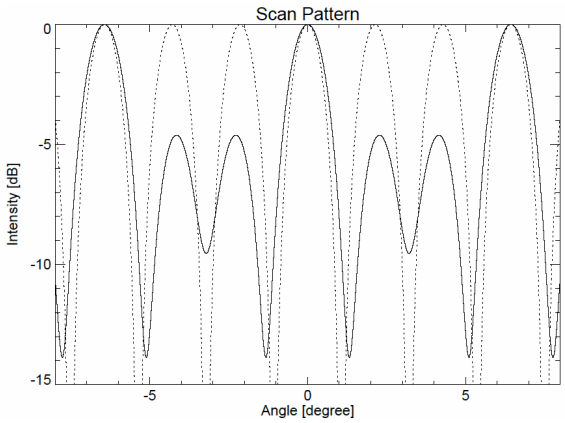

Figure 8: Scan pattern of two-antenna (dotted) and three-antenna (solid) configuration with baseline ratios 1:2:3

One possibility to exploit the additional information of the third antenna is to support the conventional phase unwrapping processes of one antenna pair by the additional information of the third antenna.

However, a vector based interpretation of the three measured complex valued image pixels of each resolution cell provides better results and additional features.

2.2.2 Pixel based elevation estimation

We estimate the elevation angle of a pixel in principle independent of any neighbour pixels on the basis of a combined evaluation of the three measured signals. The following model can be used for a pixel v of the image, which has three components according to the tree antennae.

$$\mathbf{z}_v = c_v \mathbf{a}_v(\mathbf{u}_v) + \mathbf{n}_v$$

Here, c is the complex SAR image, $\mathbf{u}$ is a unit vector to the analysed pixel, $\mathbf{n}$ is uncorrelated receiver noise and

$$\mathbf{a}(\mathbf{u}) = \begin{bmatrix} k_1(\mathbf{u})\mathrm{e}^{j\beta(\mathbf{u}\mathbf{r}_1)} \\ k_2(\mathbf{u})\mathrm{e}^{j\beta(\mathbf{u}\mathbf{r}_2)} \\ k_3(\mathbf{u})\mathrm{e}^{j\beta(\mathbf{u}\mathbf{r}_3)} \end{bmatrix},$$

where $\mathbf{r}_i$ denotes the position of sensor i and k_i comprises the two-way characteristics as well as the relative phase shifts of the i-th transmit/receive pair. $\mathbf{a}(\mathbf{u})$ is called DOA-vector (direction of arrival).

In a first step, a calibration of the system has to be carried our, i.e. $\mathbf{k}(\mathbf{u})$ has to be determined. After flat earth compensation (i.e. removing a slant range dependent phase to get the expected phase term for a topographically flat earth surface), an estimation for $\mathbf{k}$ is determined by the eigenvector corresponding to the largest eigenvalue of the covariance matrix given by the flat earth compensated signal vector $\tilde{\mathbf{z}}_v$. This leads to a calibrated representation of the signal, which, after some averaging, serves as input to a monopulse estimator. The thus estimated $\Delta\mathbf{u}$ determines the deviation of the flat earth and allows to calculate the height pixel-by-pixel by simple geometrical operations.

If we look at the eigenvalue distribution of the two largest eigenvalues λ_1 and λ_2 of the averaged signal, we expect, with the exception of some leakage out of the signal subspace by high intensities, a high λ_1 / λ_2 ratio, if only one single $\Delta\mathbf{u}$ contributes to the pixel. On the other hand, a moderate ratio will result if two $\Delta\mathbf{u}$, belonging to different heights, are mixed up within the same pixel. Thus, we are able to decide weather one pixel contains contributions from more than one scene height. The eigenvectors can be used in a subsequent step to estimate the heights which belong to the current image pixel.

3.0 MOVING TARGET INDICATION (MTI)

3.1 Properties of moving target echoes

Moving objects pose problems in conventional SAR since the relative motion between the radar sensor and the scene behaves no longer as presumed originally. SAR processing of acquired moving target echoes leads to defective images of the targets: misplaced in the resulting image, defocused or not appearing at all.

The problem can be formalised similar to SAR imaging. A sensor moves along the x-axes with a constant

velocity. A target at position (x_t, y_t) moves in arbitrary direction with also constant velocity. The distance and the direction from the sensor to the target depend on slow-time and the target parameters ϑ. Figure 9 depict the situation.

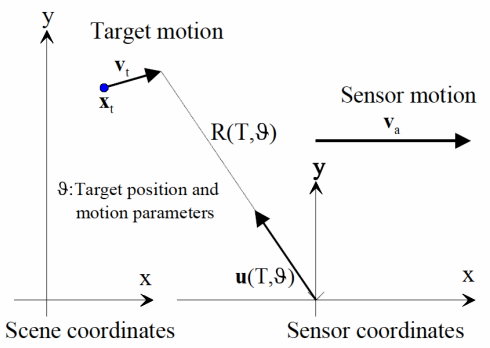

Figure 9: Geometry for a SAR constellation with a moving target.

Analysing recorded raw data in slow-time incorporates different parameters: time, range and frequency. While two-dimensional presentations of the data in range and frequency, range and time as well as in time and frequency are commonly used, a three dimensional illustration like depicted in Figure 10 is seldom presented. The appearance of the relation depends on all target parameters. However, the parameters cannot be unambiguously determined from the course of the data.

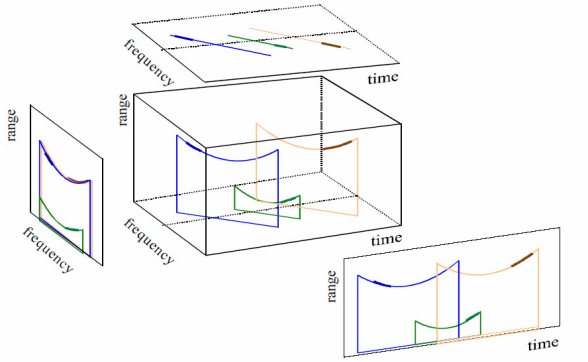

Figure 10: Three-dimensional SAR data representation.

Consequences of unconsidered motion of targets in conventional SAR imaging is illustrated in Figure 11. Radial motion only causes a shift of the Doppler band. The slope of the Doppler history remains unchanged, thus the matched filter compresses the echo of the target to a small object. Because of the shifted Doppler spectrum a portion of the signal energy will not contribute to the image so the target response will be decreased. Since the Doppler modulation is approximately linear, the shift in Doppler domain corresponds to a shift in range direction. The radial motion thus also results in a range offset of the imaged target. Echoes of a target which moves parallel to the flight path have a Doppler slope which deviates from the slope of clutter objects. The commonly used matched filter is not able to compress such a target, because uncompensated phase fluctuation remains after the matched filter process. Anti-parallel motion leads to a similar effect. If a target has a radial component which shifts the Doppler frequency history out of the processed clutter band, it will not be imaged.

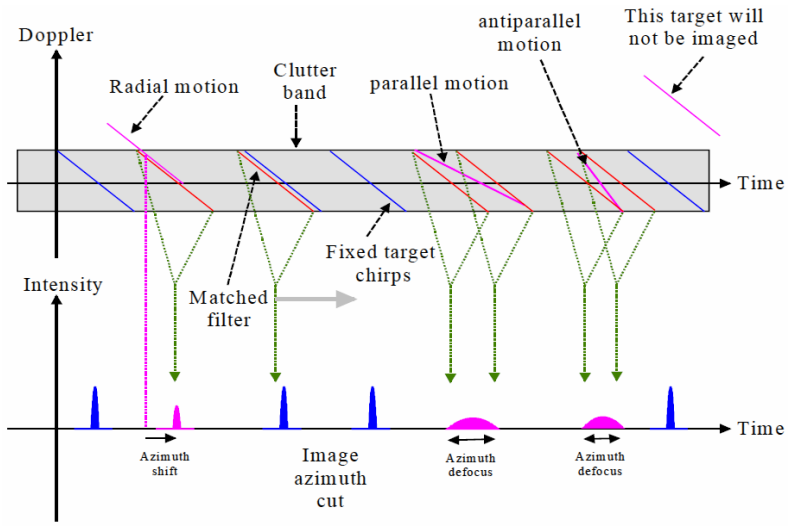

Figure 11: Effects of motion in SAR imaging.

A couple of heuristic approaches exist to cope with moving targets using a conventional single channel SAR system:

- Detection outside the clutter bandwidth
- Chirp slope analysis
- Chirp filter bank
- MTI via multilook images (change detection)
- Range walk detection
- Chirp offset detection
- Reflectivity displacement method
- Relation to context:
  - Shadow detection
  - Off-road detection

However, these methods exhibit weaknesses particularly for fast and slowly moving targets and for low SNR. Efficient MTI capability is only obtainable using multiple channels in flight direction.

3.2 Multichannel MTI

Figure 12 illustrates the idea of multichannel MTI and the realisation concept in the SAR context. Image a) depicts the displaced phase centre antenna technique (DPCA): two antennae installed at different positions of the sensor platform acquire radar data, using the same geometry (determined by the antenna position at pulse acquisition instant) but at different moments. Obviously, fixed targets produce identical echoes, thus they cancel out in the difference signal. Remaining energy is caused by objects with radial motion and noise. DPCA is very illustrative but can only be used in extended variants. SAR data of a two-antenna system, like it is depicted in b), can be exploited by along-track interferometry. In a first step, a complex SAR image will be calculated for each channel. Afterwards, the images will be multiplied complex conjugated. The remaining phase indicates radial motion of moving targets. For fixed targets the resulting phase vanishes. A result of along-track interferometry is shown in Figure 13. To improve the MTI capability, more antennae have to be used. Figure c) depicts this technique. The acquired data

represent samples of the wave field in space and time. With the aid of space time adaptive processing (STAP) a couple of motion information can be calculated out of the data.

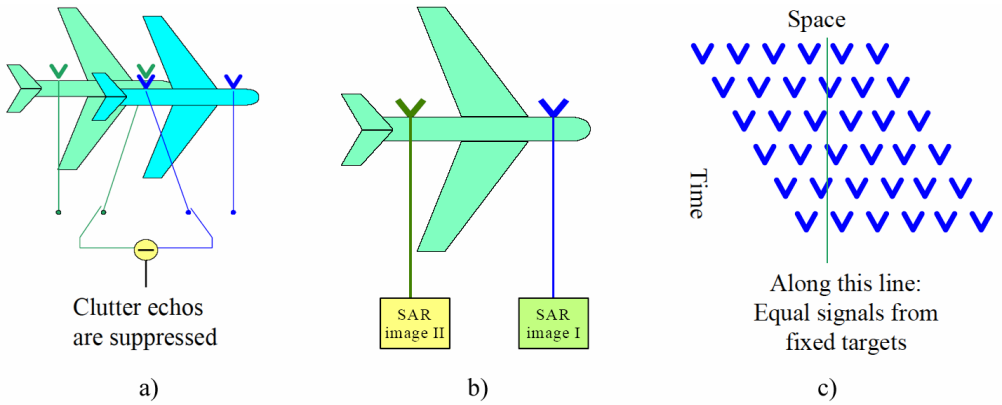

Figure 12: Ideas for multichannel MTI processing: a) displaced phase centre antenna (DPCA), b) application of DPCA to SAR case, c) extension of the principle to space time adaptive processing (STAP)

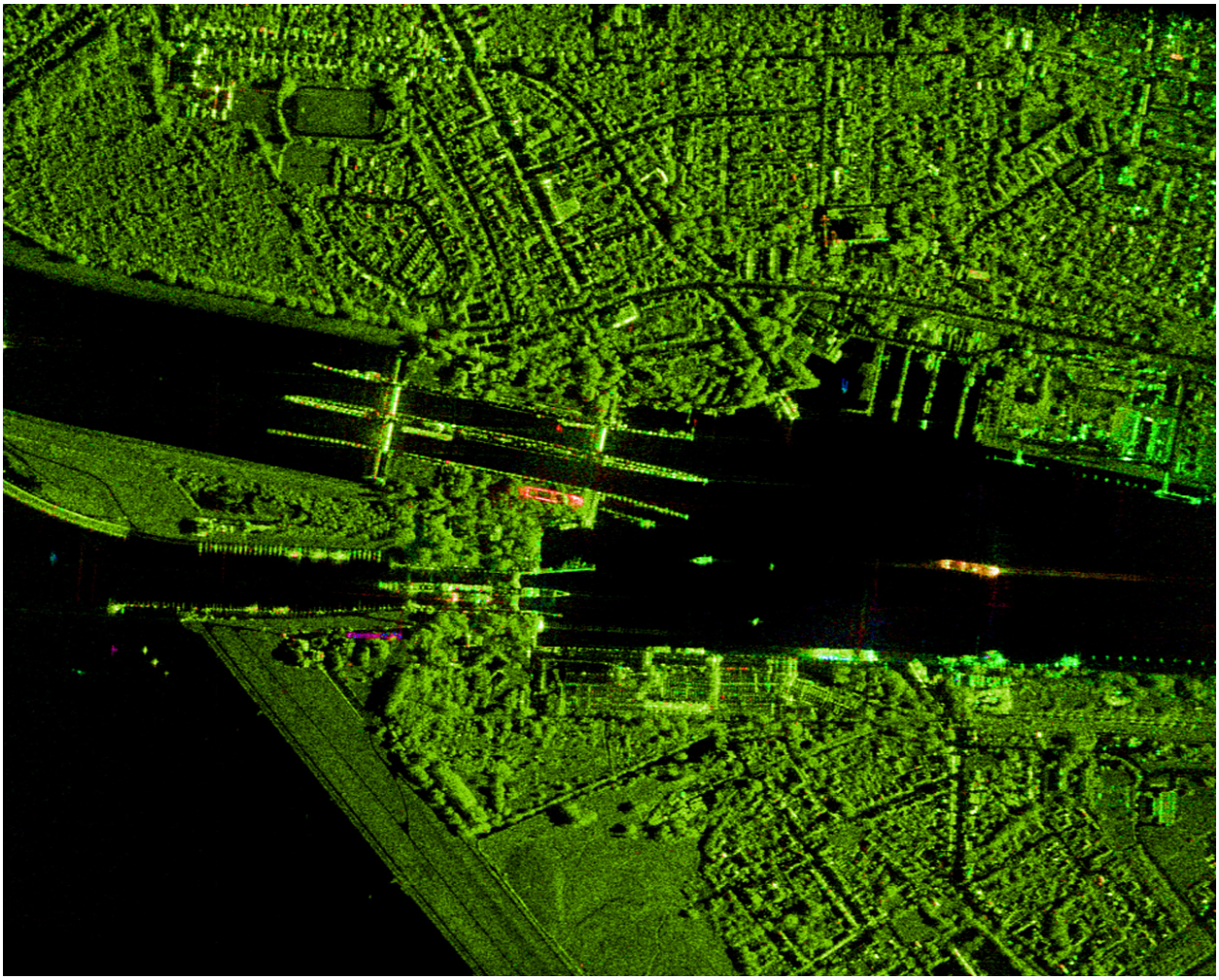

Figure 13: Along-track interferometry of the ship lock Brunsbüttel. The image colour is chosen according to the differential phase of the two SAR images.

4.0 LITERATURE

[1] S. Barbarossa and A. Farina, Space-time-frequency processing of synthetic aperture radar signals, IEEE Trans. Aerospace Electronic Systems, vol. 30, no. 2, pp. 341-358, 1994

[2] W. G. Carrara, R. S. Goodman and R. M. Majewski, Spotlight Synthetic Aperture Radar: Signal Processing Algorithms, Artech House, Norwood, MA, 1995

[3] D. Carrasco, J. Diay and A. Broquetas, Wide area interferometry with ERS-1, Proc. EUSAR´96, pp. 177-180, Königswinter, Germany, 1996

[4] J. Ender, Space-time processing for multichannel synthetic aperture radar, Electro. & Commun. Eng. Journal, Feb. 1999, pp. 29-38

[5] J. H. G. Ender, The meaning of k-space for classical and advanced SAR-techniques, in Proc. PSIP´2001, 2001

[6] J. H. G. Ender and A. R. Brenner, PAMIR – a wideband phased array SAR/MTI system, in Proc. EUSAR 2002, pp. 157-162, 2002

[7] J. H. G. Ender, SAR/MTI with multi-subaperture phased arrays, 2003 Tyrrhenian International Workshop on Remote Sensing (TIWRS 2003), Elba Island, Italy

[8] W. Hong, Y. Huang and S. Mao, A comparison of several spotlight SAR algorithms, AEÜ Intern. Journal of Electronics and Comm., vol. 50, no. 2, pp. 127-132, 1996

[9] F. Lombardini, Absolute phase retrieval in a three-element synthetic aperture radar interferometer, SIE-ICR 96, International Radar Conference, pp. 309-312, 8-11 Oct. 1996, Beijing, China

[10] P. Lombardo and F. Lombardini, Multi-baseline SAR interferometry for terrain slope adaptivity, IEEE Proc. Nat. Radar Conf. 1997, pp. 196-201, New York, 1997

[11] R. T. Lord and M. R. Inggs, High range resolution radar using narrow linear chirps offset in frequency, in Proc. of the 1997 South African Symp. on Comm. and Signal Proc., pp. 9-12, 1997

[12] C. Prati, A. M. Guarnieri and F. Rocca, Spot mode SAR focusing with the $\omega - k$ technique, in Proc. IGARSS´91, pp. 632-634, 1991

[13] L. Rößing and J. H. G. Ender, Advanced SAR interferometry techniques with AER-II, Int. Radar Symp. IRS´98, Munich, Germany, 1998

[14] L. Rößing and J. H. G. Ender, Multi-antenna SAR tomography using super resolution techniques, Frequenz 55, 3-4, pp. 123-128, 2001

[15] M. Soumekh, Synthetic Aperture Radar Signal Processing with MATLAB Algorithms, Wiley-Interscience, New York, 1999

[16] A. F. Yegulalp, Fast backprojection algorithm for synthetic aperture radar, in The Record of the 1999 IEEE Radar Conference, pp. 60-65, 1999